Sensors and Materials, Vol. 35, No. 4 (2023) 1241–1254
MYU Tokyo

S & M 3242

Optimization of Displacement by Fluid–Solid Coupled Vibration of Hydraulic Hoses

Tian-Syung Lan,[1,2*] Huo Wang Zhang,[2] Zhi Wei Zhang,[2]
Xuan-Jun Dai,[2] and Yingchun Long[1**]

[1]School of Intelligent Engineering, Shaoguan University, Guangdong 512005, China
[2]College of Mechanical and Control Engineering, Guilin University of Technology, Guangxi 541004, China

(Received September 12, 2022; accepted February 14, 2023)

Keywords: vibration optimization, Taguchi experiment, hydraulic hose, response surface analysis

Under the excitation of hydraulic oil, fluid–structure coupling affects a hydraulic hose. We analyzed the vibration characteristics and optimized the parameters of the vibration of a hydraulic hose. SolidWorks was used to model a three-layer steel wire wound around a polytetrafluoroethylene (PTFE) hose. A two-way fluid–structure coupling model was built to analyze the influence of different parameters on the displacement by vibration and the fluid vibration speed. A three-factor and three-level Taguchi experiment with displacement was carried out to verify the influence of the parameters. In the analysis of the response surface, fitting regression was conducted using the Box–Behnken method to analyze the vibration displacement. The optimal predicted parameters were a winding angle of 53.8384°, a wall thickness of 7.31313 mm, and a bending radius of 164.343 mm. The error between the predicted and simulated values was ±3.5% for the optimized parameters and the displacement was reduced by 47% for the optimal parameters. The optimal parameters can be used as reference values to improve the working life of vibrating hydraulic hoses in future studies on the vibration characteristics of hydraulic hose systems.

1. Introduction

The vibration of a hydraulic hose by internal fluid flow causes movement and deformation of the inner wall and the hose by producing fluctuations in the fluid movement. Such phenomena are mutually reciprocating, generating a coupling effect between the fluid and the hydraulic pipeline. The interface between the fluid and the solid is the main location of the fluid–solid interaction that initiates the phenomena.

To carry out research related to these phenomena, various data are required for analysis. Such data include the radius of the hose and the viscosity and density of the fluid moving in the hose.(1) Sensor data such as the pressure,(2) temperature, vibration, and velocity of the fluid and the deformation and frequency of the pipeline(3) are also required. The development of sensor technology has contributed considerably to the study of fluid characteristics with easier data

*Corresponding author: e-mail: tslan888@yahoo.com.tw
**Corresponding author: e-mail: sgulyc@139.com
https://doi.org/10.18494/SAM4118

ISSN 0914-4935
https://myukk.org/

acquirement.[4] On the basis of the data, many researchers have conducted related studies as follows.

Kutin and Bajsic studied the mechanism of the change in the fluid velocity load and improved a coupling vibration model of the fluid structure.[5] Talemi *et al.* conducted a numerical simulation of the dynamic ductile fracture of steel pipes by combining fluid dynamics with the deformation fracture mechanism.[6] Keramat *et al.* analyzed pressure data collected from oil pipelines in the time and frequency domains and considered fluid–structure coupling. They explained the pressure fluctuation using the Poisson coupling.[2] Daude *et al.* proposed Euler/homogeneous equilibrium model equations for 1D and 3D finite volume coupling to overcome the inherent limitations of 1D modeling.[7] Zhang *et al.* proposed a numerical coupling solution between the hydraulic capsule pipeline transport domain and the fluid domain in a pipeline based on the bidirectional fluid–structure coupling method.[8] Qu *et al.* established the motion equation of a hydraulic composite pipe by using random vibration and fluid–structure coupling to understand the stochastic vibration excited by white noise. The effects of external excitation, fluid velocity, fluid pressure, and structural parameters on the stress of a composite pipe were also studied.[9] Xu *et al.* established a finite element model of tubing corrosion based on the corrosion mode, fluid–structure coupling, and the influence of sand to clarify the relationship between the tubing corrosion law and failure areas.[1] Duan *et al.* simulated and analyzed modal changes of dry and wet single pipelines and discussed the influence of the fluid–solid coupling effect, inlet pressure, and ambient temperature on the tubing.[3]

In the literature review, improvements were found in the convection–solid coupling calculation method. In terms of methodology, the finite element method (FEM) has been mainly used to study the coupling vibration of straight round, T-shaped, conical, and bending pipes. However, there has been limited research on the theoretical analyses or on the coupling vibration and fluid–structure coupling of straight and elbow pipes. The parameters affecting the vibration of the hose have also not been studied extensively. Therefore, we optimized the parameters of the vibration of a hydraulic hose through analysis of the vibration characteristics. A two-way fluid–structure coupling model was proposed to clarify the influence of various parameters on the displacement by vibration and the fluid vibration speed. The optimal parameters proposed in this study can be used as a basis for further studies to describe the vibration of hydraulic hoses.

2. Finite Element Vibration Analysis Based on ANSYS Workbench

2.1 Materials

We used a 2SN06 hydraulic hose in this study.[10] The dimensions of the hydraulic hose and its steel wire are respectively shown in Tables 1 and 2. SolidWorks was used to model the fluid characteristics of the hydraulic U-shaped hose as shown in Fig. 1.

Table 1
Dimensions of 2SN06 hydraulic hose (in mm).

Model	Nominal diameter	Inner diameter	Outside diameter	Minimum bending radius
2SN06	10	9.5	19.1	130

Table 2
Dimensions of winding wire of 2SN06 hydraulic hose.

Number of layers	Wire diameter (mm)	Modulus of elasticity (MPa)	Tensile strength (MPa)	Poisson's ratio	Working pressure (MPa)
3	0.4	200	2000	0.3	20

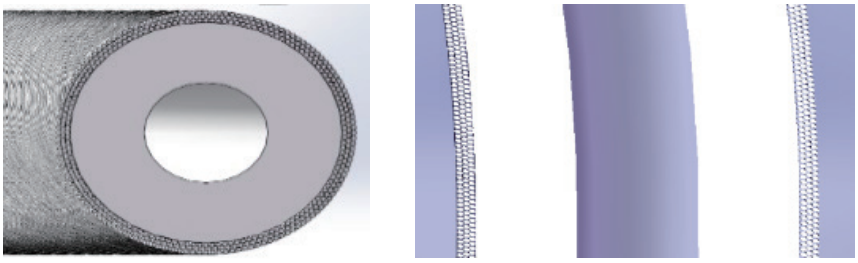

Fig. 1. (Color online) Hydraulic U-shaped hose used in this study.

Table 3
Frequency of the hose and the coupled frequency of the fluid and hose in each mode (Hz).

Mode	Empty hose	Fluid and hose
1 (natural frequency)	224.70	114.85
2	490.77	251.52
3	623.88	318.25
4	1148.90	588.13
5	1319.80	672.80
6	2145.50	1097.3
7	2259.80	1152.2
8	3271.40	1671.7

2.2 Vibration characteristics of hydraulic hose

Table 3 shows the natural frequency of the hydraulic hose and the coupled frequency of the fluid (oil) and hose. The frequency increased with the mode number as shown in Table 3. As the frequency of the empty hose increased, the frequency of the fluid and hose also increased. However, the frequency of the fluid and hose was lower than that of the empty hose. This indicates that the fluid in the hydraulic hose reduced the frequency of the U-shaped hose containing the fluid. Resonance mainly occurred in mode 1.[11]

The analysis of the vibration of the empty hose and the fluid and hose in each frequency mode was carried out in ANSYS Workbench. The result is shown in Fig. 2. In mode 1, a swing in the *X*-direction is observed with a maximum displacement of 90.038 mm. This is the largest displacement among the eight modes with different frequencies. In mode 2, a swing in the *Y*-direction and slight torsion in the *X*-direction are found with a maximum displacement of 69.018 mm. The torsional vibration around the middle of the hose can be seen in mode 3, where the maximum displacement of 86.864 mm occurs in the middle of the hose. The vibration mode is manifested in the tensile bending along the *Z*-axis in mode 4, and the maximum displacement occurs in the maximally bent part of the hose. Here, the maximum displacement is 89.326 mm.

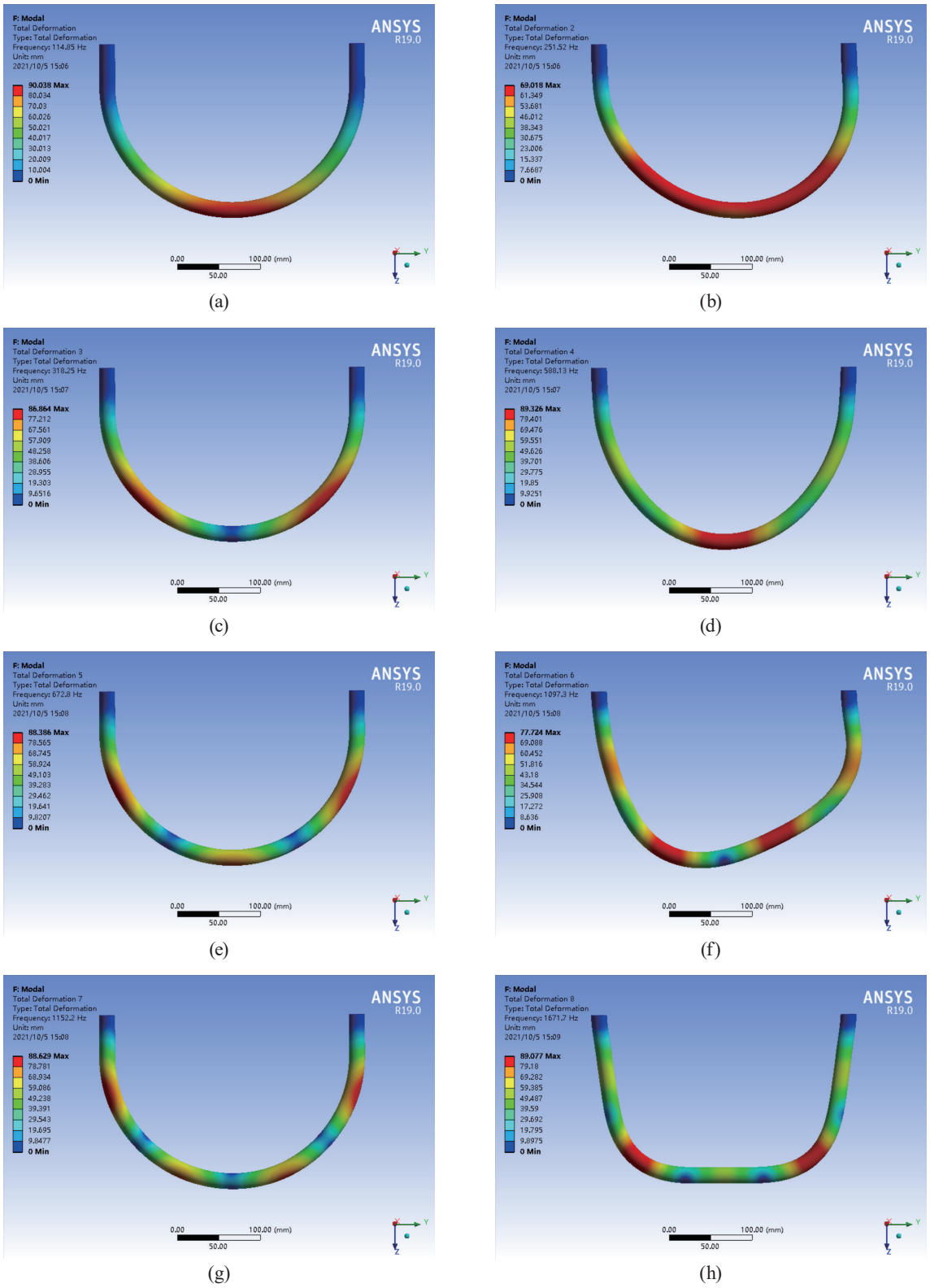

Fig. 2. (Color online) Displacement of the hose with fluid in each frequency mode. (a) First-order mode. (b) Second-order mode. (c) Third-order mode. (d) Fourth-order mode. (e) Fifth-order mode. (f) Sixth-order mode. (g) Seventh-order mode. (h) Eighth-order mode.

Three sections of torsion and bending occur at the waist and bottom in mode 5. The maximum displacement of 88.386 mm is observed at these three parts. In mode 6, bending along the *Y*-axis and torsion around the *X*-axis occur. The maximum displacement of 77.724 mm occurs at the bottom and upper parts. Torsion and bending around the whole hose are observed in mode 7 with a maximum displacement of 88.629 mm. In mode 8, two parts at the bottom show internal and external bending with torsion around the *Z*-axis. The maximum displacement of 89.077 mm occurs at the bottom part. These results show that the resonance of the hose in each mode is different and that any form of vibration can occur upon the superposition of frequency modes.

2.3 Characteristics of bidirectionally coupled vibration of fluid and hose

To explore the displacement and its velocity for the fluid and hose, the bidirectional coupling of the vibration of the fluid and hose was simulated with different flow rates, inlet pressures, bending radii of the hose, wall thicknesses, and port lengths.

Fluid–hose coupling analysis was carried out with the boundary conditions of flow rates of 5 and 7 m/s. The monitoring points were set at the boundary of the fluid–solid interface. The displacements with time in the *X*-, *Y*-, and *Z*-directions were recorded. The overall changes in the displacement with time are shown in Figs. 3 and 4 for flow rates of 5 and 7 m/s, respectively.

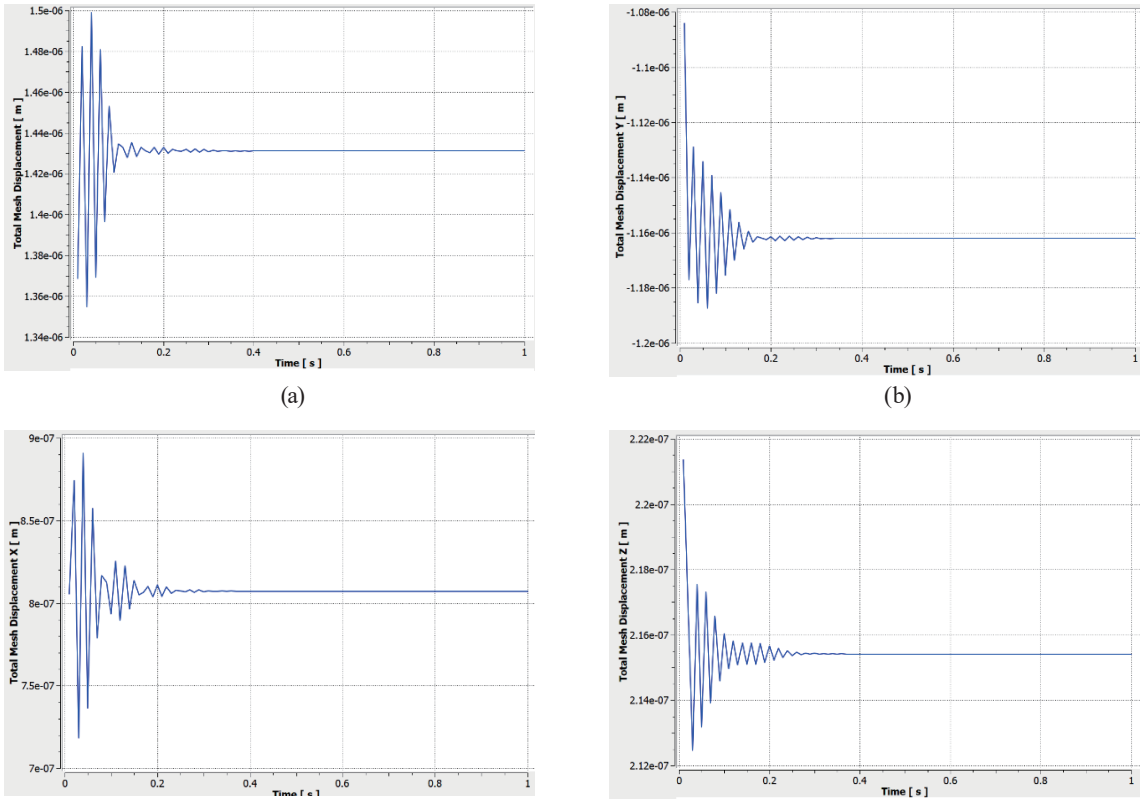

Fig. 3. (Color online) Displacement with time at a flow rate of 5 m/s. (a) Overall displacement. (b) Displacement in *X*-direction. (c) Displacement in *Y*-direction. (d) Displacement in *Z*-direction.

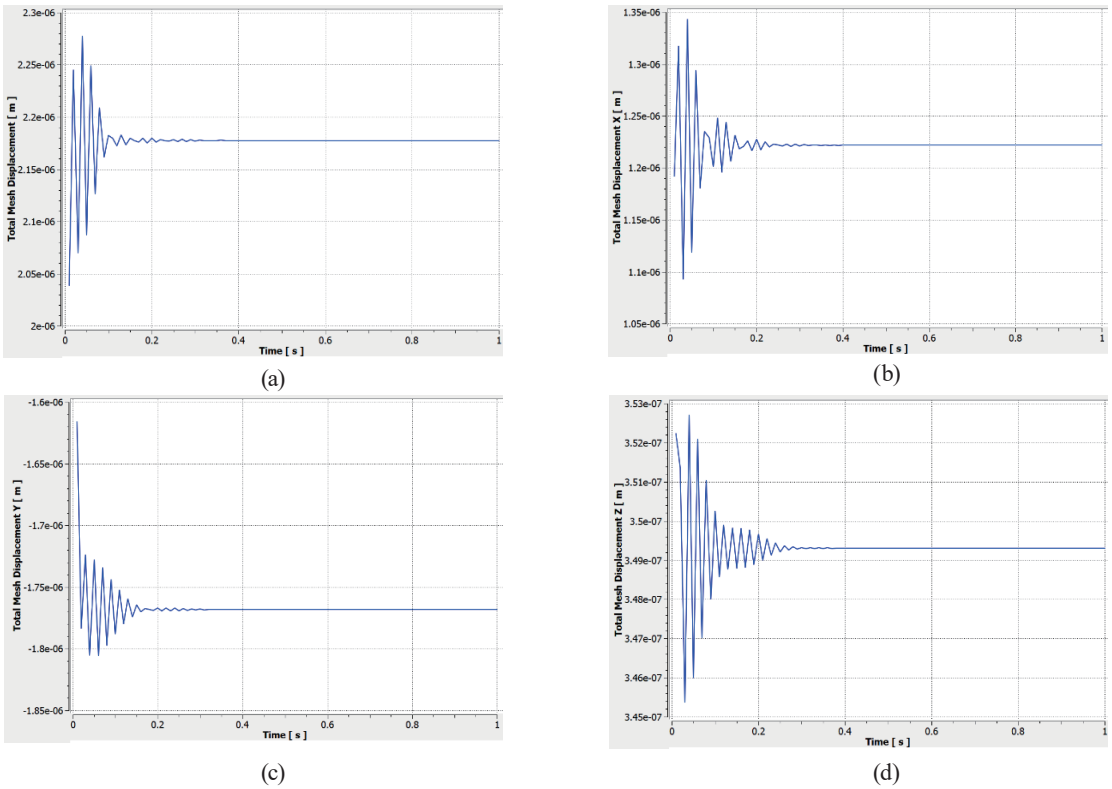

Fig. 4. (Color online) Displacement with time at a flow rate of 7 m/s. (a) Overall displacement. (b) Displacement in *X*-direction. (c) Displacement in *Y*-direction. (d) Displacement in *Z*-direction.

At the moment of fluid injection into the hose, the displacement induced by vibration in each direction generates a larger displacement. Then, the displacement decreases continuously and is finally stabilized with little displacement. An increase in the flow rate causes the displacement and amplitude of the hose to increase in each direction. The maximum displacements in the *Y*-direction are -1.19×10^{-6} and -1.81×10^{-6} m at the flow rates of 5 and 7 m/s, respectively. The maximum displacements in the *X*-direction are 1.73×10^{-7} and 2.50×10^{-7} m, respectively. Therefore, the vibration of the hose with the fluid injection in the *X*- and *Y*-directions mainly affects the displacement of the hose.

The relationship between the velocity of displacement and time in the *X*-, *Y*-, and *Z*-directions at the monitoring points at flow rates of 5 and 7 m/s are shown in Figs. 5 and 6, respectively. The velocity in each direction at the monitoring point tends to be stable after displacement induced by vibration, and the vibration amplitude becomes smaller over time. After the vibration stops at about 0.3 s, little displacement is observed. When the inlet velocity of the displacement increases, the amplitude of the displacement also increases. The velocity of the displacement in the *Y*-direction is the highest and is -2.15×10^{-4} and -3.21×10^{-4} m/s at the flow rates of 5 and 7 m/s, respectively. The maximum velocity in the *Y*-direction is 4.05×10^{-4} and 5.98×10^{-4} at the flow rates of 5 and 7 m/s, respectively.

It is concluded that the flow rate has a significant impact on the coupled vibration of the fluid and hose. Increasing the flow rate aggravates the coupled vibration of the fluid and hose.

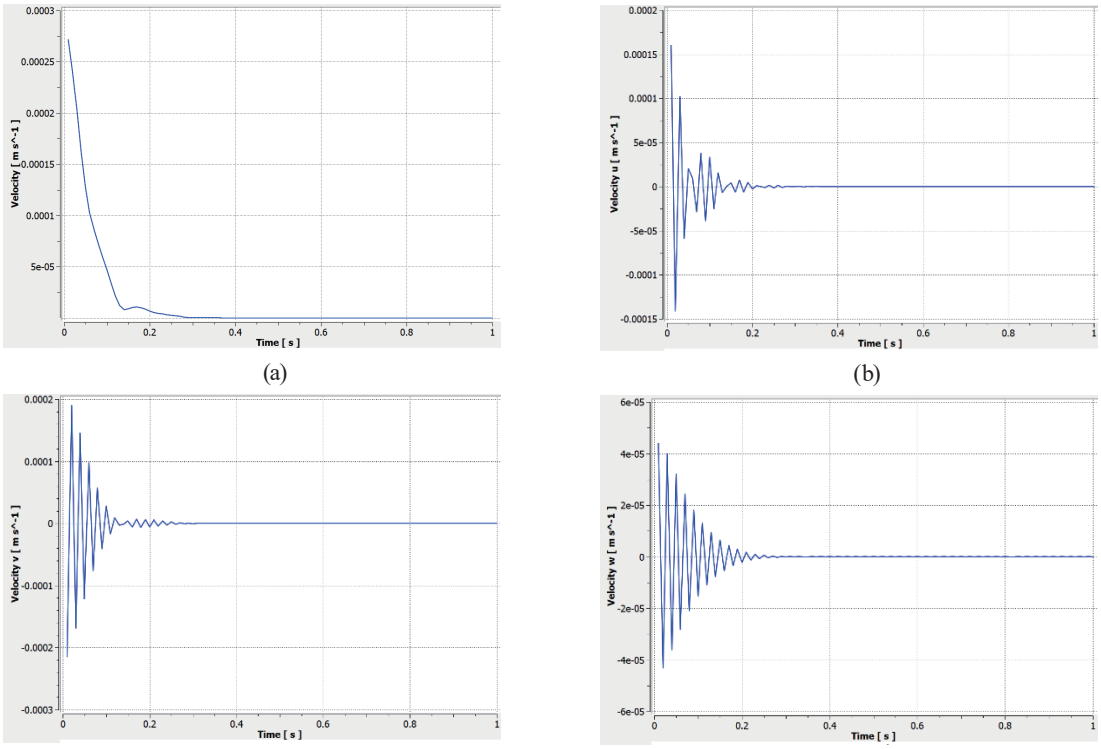

Fig. 5. (Color online) Velocity and time at a flow rate of 5 m/s. (a) Overall velocity change with time. (b) Velocity change in *X*-direction. (c) Velocity change in *Y*-direction. (d) Velocity change in *Z*-direction.

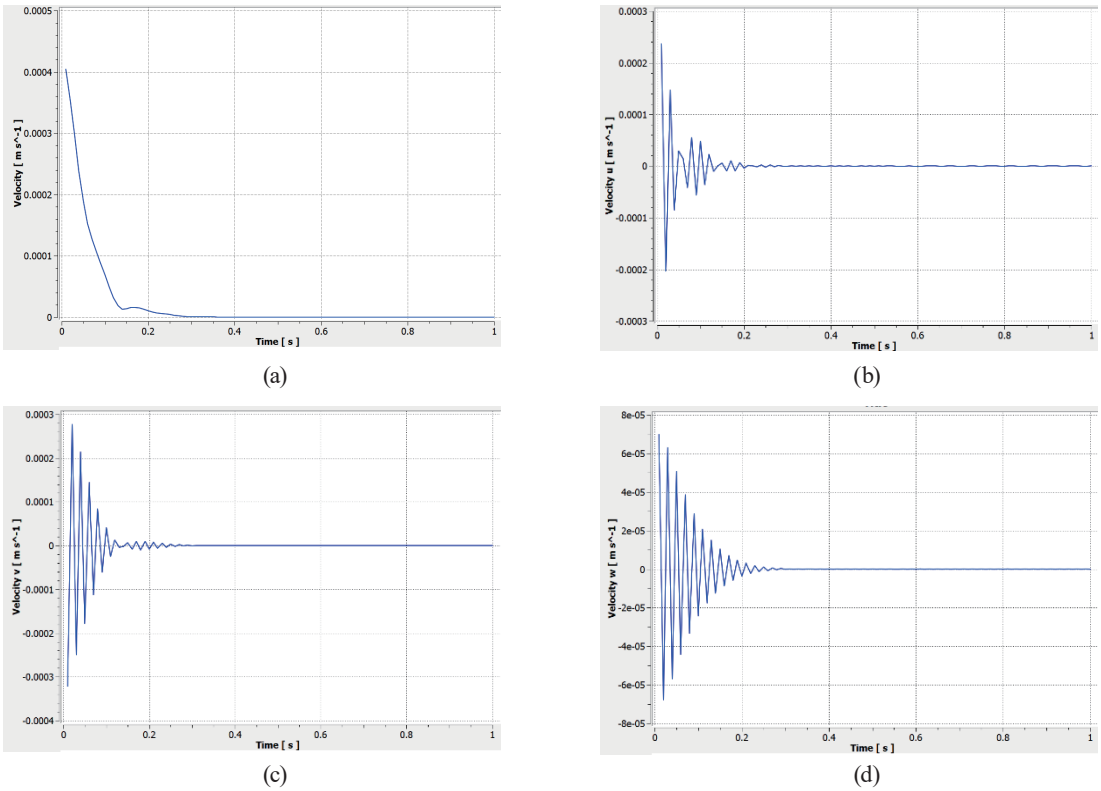

Fig. 6. (Color online) Velocity and time at a flow rate of 7 m/s. (a) Overall velocity change with time. (b) Velocity change in *X*-direction. (c) Velocity change in *Y*-direction. (d) Velocity change in *Z*-direction.

We also simulated the changes in displacement for different inlet pressures, bending radii, and port lengths. At inlet pressures of 10 and 12 MPa, the displacement induced by the vibration of the hose was reduced with the decrease in inlet pressure. The wall thickness also affected the displacement of the fluid and hose, because the hose with a thickness of 6 mm showed a larger displacement than that of the hose with a thickness of 8 mm. For the fluid and hose with a port length of 30 mm, the displacement was larger in the *X*-direction than in the *Y*- and *Z*-directions, but it was larger in the *Y*- and *Z*-directions than in the *X*-direction for a port length of 50 mm. Increasing the port length increased the velocity of displacement in the *X*- and *Y*-directions. The velocity in the *Z*-direction did not show a significant difference for the two port lengths. Therefore, the effect of the port length on the coupled vibration of the fluid and hose was unclear.

3. Field Test of Hydraulic Hose Performed Using Minitab

3.1 Taguchi experiment

The influence of the length of the straight part of the hydraulic hose on the coupled vibration was not observed in the simulation. Thus, we carried out an experiment using the Taguchi method to determine the influence. As the displacement due to the vibration of the hose is mainly caused by the coupling effect of the fluid and hose, the displacement due to the vibration of the hose was taken as the response value in the Taguchi experiment. The controlling parameters were the wall thickness (A), bending radius (B), and port length (C) of the hose. Three different values were set for each parameter for the orthogonal design of the experiment. The L_9 orthogonal array was used for a simulation experiment of the coupled vibration of the fluid and hose in ANSYS Workbench. The displacement by vibration at the monitoring points was calculated as a response value using the ANSYS computational fluid dynamics (CFD) method. The parameters are shown in Table 4.

3.2 Analysis of variance

Variance analysis of the Taguchi analysis data for vibration was performed to verify the significance of the parameters as shown in Table 5. Our null hypothesis is that all factors have no significant effect on displacement by vibration, and we employed a confidence interval of 95%. When $P < 0.05$, the original hypothesis was not accepted, which allowed us to conclude the significant effect of the parameter on the response value. Table 5 shows that the *P* values of the wall thickness and bending radius of the hose are less than 0.05, indicating that they have

Table 4
Three different levels of the three parameters (mm).

Level	Wall thickness (A)	Bending radius (B)	Port length (C)
1	6	150	10
2	7	160	15
3	8	170	20

Table 5
Variance analysis result in the Taguchi experiment.

Parameters	Sequential sum of squares	Adjusted sum of squares	Adjusted mean square	*F*	*P*
Wall thickness	18.8138	18.8138	9.4069	117.17	0.008
Bending radius	31.2694	31.2694	15.6347	194.75	0.005
Port length	0.0692	0.0692	0.0346	0.43	0.699
Residual error	0.1606	0.1606	0.0803		
Total	50.3130				

significant effects on the response value. The *P* value of the port length is higher than 0.05, indicating that the port length has no significant effect.

4. Parameter Optimization Based on Response Surface Methodology

4.1 Response surface methodology

The Box–Behnken design in the response surface methodology was used to set each experimental point at each midpoint of cube edges.[12] The three-factor Box–Behnken points used in this study are shown in Fig. 7.

4.2 Establishment of response surface model

According to the results of the Taguchi experiment, there was no obvious influence of the port length of the hose on the displacement by vibration. Therefore, in the response surface analysis, the port length was eliminated. Instead, the winding angle of the steel wire of the hose was introduced as a new factor. The winding angle was recombined with the wall thickness and bending radius to design a three-factor and three-level experiment to explore their influences on displacement. The Box–Behnken method and ANSYS Workbench were used in the simulation experiment. The results are shown in Table 6.

Primary and quadratic regression analyses were performed to clarify the relationship between the wall thickness, bending radius, winding angle of the steel wire of the hose, and vibration displacement. Figures 8 and 9 respectively show the normal probability diagram and histogram obtained from primary and quadratic regression, respectively. Tables 7 and 8 present

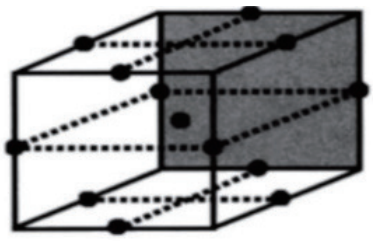

Fig. 7. Schematic diagram of three-factor Box–Behnken points.

Table 6
Factors for Box–Behnken experimental design.

Order	Point type	Winding angle (°)	Wall thickness (mm)	Bending radius (mm)	Displacement (mm)
1	2	50	6	160	0.0030
2	2	60	6	160	0.0036
3	2	50	8	160	0.0018
4	2	60	8	160	0.0026
5	2	50	7	150	0.0025
6	2	60	7	150	0.0033
7	2	50	7	170	0.0017
8	2	60	7	170	0.0019
9	2	55	6	150	0.0031
10	2	55	8	150	0.0024
11	2	55	6	170	0.0029
12	2	55	8	170	0.0018
13	0	55	7	160	0.0013

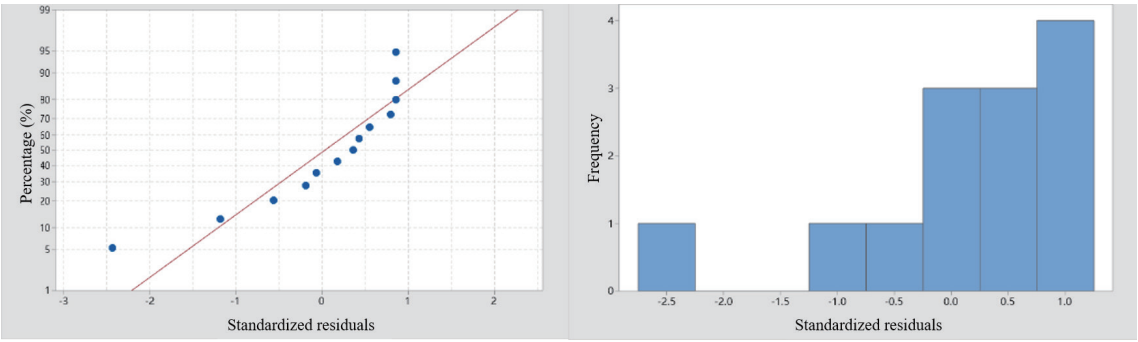

Fig. 8. (Color online) Normal probability diagram and corresponding histogram obtained by primary regression.

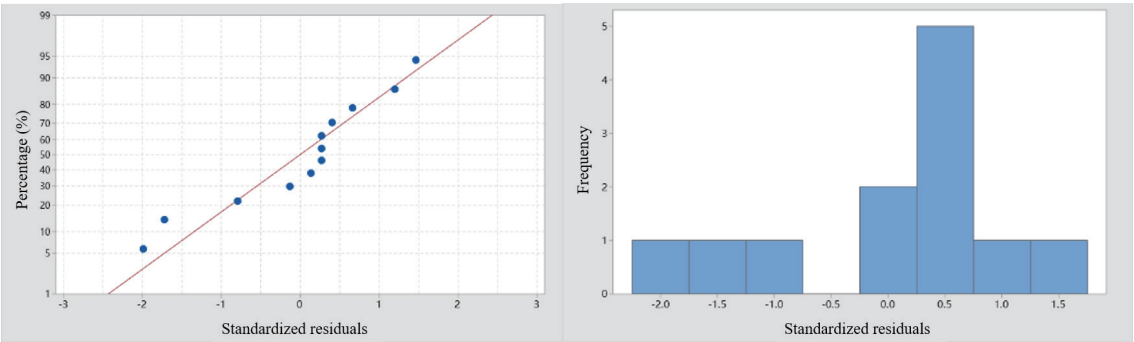

Fig. 9. (Color online) Normal probability diagram and corresponding histogram obtained by quadratic regression.

the statistics obtained from the regression. The fitting of the primary linear regression model is not significant, while the quadratic regression model fits better with the statistics. According to the analysis of variance, the P value of the model is 0.003 (<0.05), which further verifies the reliability of the quadratic regression model.

Table 7
Statistics of the primary regression model.

Standard error	R^2	Adjusted R^2	Predicted R^2
0.0004930	63.74%	51.65%	42.78%

Table 8
Statistics of the quadratic regression model.

Standard error	R^2	Adjusted R^2	Predicted R^2
0.0002661	92.95%	85.91%	82.65%

4.3 Response surface analysis

Minitab software was used to create a curved surface and draw contour lines for the three-factor and three-level experimental model based on the steel wire winding angle, wall thickness, and bending radius of the hose. The response surface diagram provides information on the factors through the shape of its surface: the greater the curvature, the greater the bending degree, indicating that the interaction between factors is significant. The contour map presents the influence of each factor on displacement by vibration to reveal the interactions between two factors and their strength. When the contours are round, the interaction between the two factors is not significant, while when the contours are elliptical, there is a significant interaction between the factors. Figure 10 shows contour maps for the winding angle of the steel wire and the wall thickness of the hose with a fixed bending radius of 160 mm, while Fig. 11 presents contour maps for the winding angle and the bending radius of the hose with a fixed wall thickness of 7 mm. Figure 12 shows contour maps for the wall thickness and the bending radius of the steel wire with a fixed wall thickness of 7 mm. No significant interaction was found between the winding angle and wall thickness, as indicated by the circular contours. In contrast, the winding angle and bending radius, and the wall thickness and bending radius have significant interactions, as indicated by their more elliptical contours. The contour maps reveal that the winding angle and bending radius of the hose are the parameters with the most significant interaction.

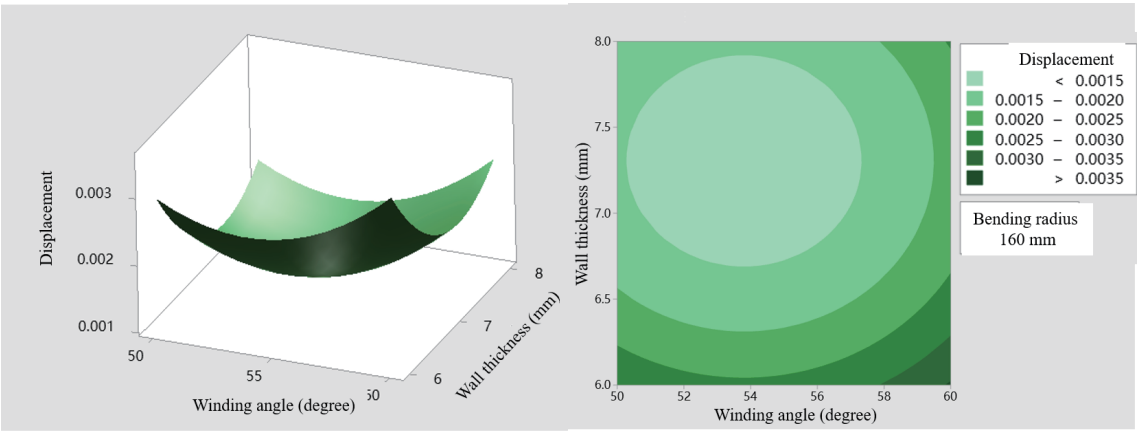

Fig. 10. (Color online) Contour map for the wall thickness and winding angle of the hose.

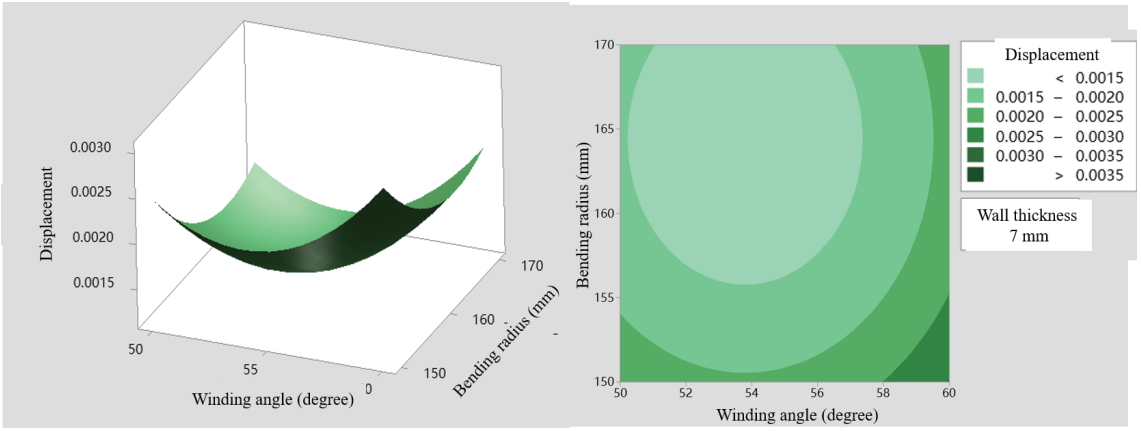

Fig. 11. (Color online) Contour map for the winding angle and bending radius of the hose.

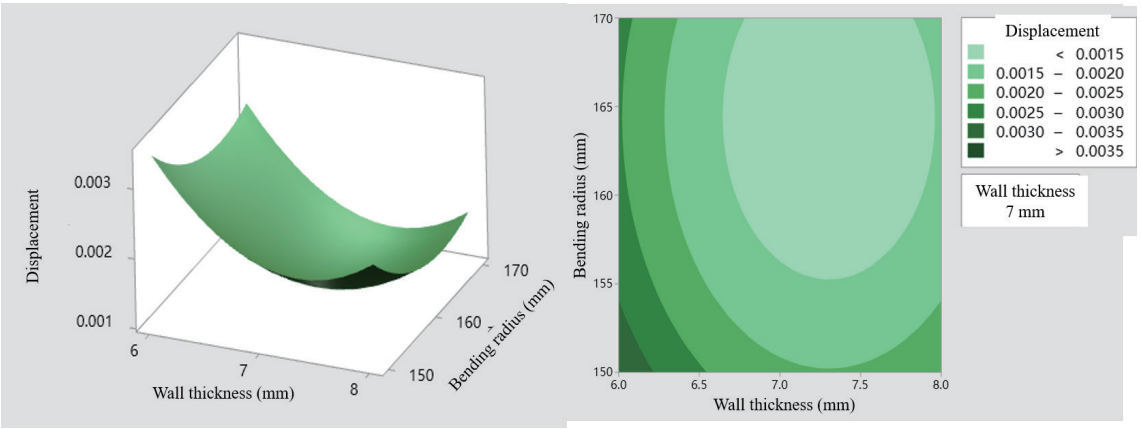

Fig. 12. (Color online) Contour map for the wall thickness and bending radius surface of the hose.

In Minitab, the response optimizer was used to predict the model parameters based on the parameters and the results of the Taguchi method and response surface analysis. The predicted results are shown in Fig. 13. The optimal parameters for the winding angle, wall thickness, and bending radius are 53.8384°, 7.3131 mm, and 164.343 mm, respectively. From these values, we find that the displacement by vibration has a minimum value of 1.106×10^{-3} mm with a standard error of 2.28×10^{-4} mm and a confidence interval at a confidence level of 95% of (5.47×10^{-4}, 1.664×10^{-3}). The prediction error at the same confidence level is (2.48×10^{-4}, 1.964×10^{-3}; Table 9).

A simulation was carried out using the FEM with the predicted parameters. The simulated displacement was 1.145×10^{-3} mm, which was 3.5% lower than the predicted value and 1.035×10^{-3} mm less than the measured displacement of 2.18×10^{-3} mm. The reduction in the displacement was 47%. These results demonstrate that the response surface methodology with the Taguchi method closely fits the displacement by the coupled vibration of the fluid hose with high reliability (Table 10).

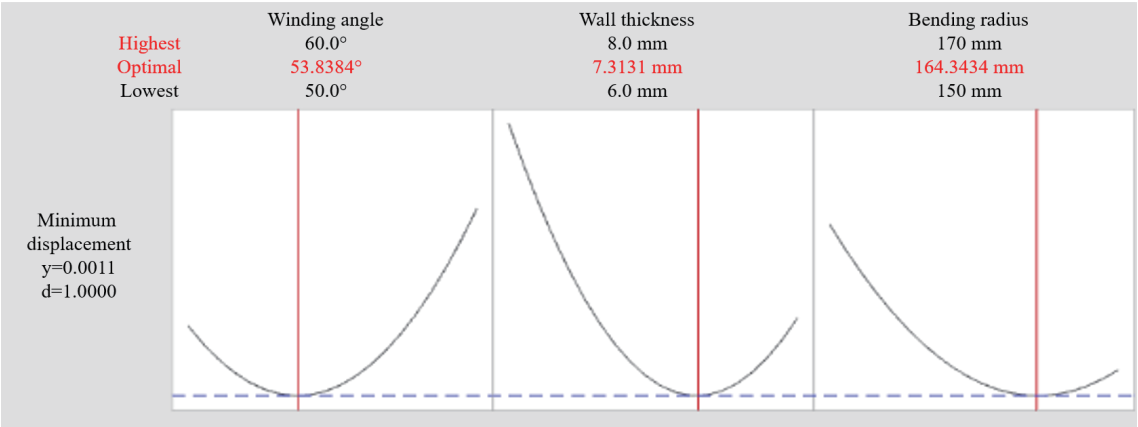

Fig. 13. (Color online) Prediction results.

Table 9
Predicted results from the response optimizer.

Winding angle (°)	53.8384
Wall thickness (mm)	7.31313
Bending radius (mm)	164.343
Vibration displacement (mm)	1.106×10^{-3}
Standard error of fitting value	2.28×10^{-4}
Confidence interval (95%)	$(5.47 \times 10^{-4}, 1.664 \times 10^{-3})$
Prediction error (95%)	$(2.48 \times 10^{-4}, 1.964 \times 10^{-3})$

Table 10
Result of prediction by response surface analysis.

Response prediction of displacement (mm)	1.106×10^{-3}
Simulated displacement (mm)	1.145×10^{-3}
Difference (mm)	3.9×10^{-5}
Difference (%)	3.5
Measured displacement (mm)	2.18×10^{-3}
Reduction in displacement (%)	47

5. Conclusion

The vibration of hoses and pipes, and the resulting displacement and deformation, affects their durability and working life. Therefore, the minimization of the displacement caused by the vibration of hoses and pipes has attracted much research interest. Such research is usually carried out through simulations and predictions, which must be based on measured data such as the pressure, temperature, vibration, and velocity of the fluid flow, as well as the deformation and frequency of the hose and pipe. Therefore, sensor technology and sensor data are required for efficient and precise research results.

We performed a comprehensive study on the displacement by the vibration of a U-shaped hydraulic hose by considering the coupling effect of the fluid and hose. The natural frequency decreases under the coupling effect. However, it is necessary to consider parameters such as the

bending radius, wall thickness, steel wire winding angle, fluid flow rate, and inlet pressure for the simulation and prediction of the vibration and displacement. The results are necessary to design the hose appropriately and effectively maintain a hydraulic hose system.

We performed a Taguchi experiment to demonstrate that the wall thickness and bending radius of the hose had a significant effect on the response value (displacement). Using the response surface methodology, we found the optimized parameters for the bending radius, wall thickness, and steel wire winding angle of the hose, assuming the coupling effect of the fluid and hose on the displacement caused by the vibration of the hose. We found that there was no significant interaction between the winding angle and wall thickness of the hose, whereas there was a certain interaction between the winding angle and bending radius and between the wall thickness and bending radius. The interaction between the wall thickness and bending radius was the most significant. The prediction and simulation results showed that the optimal winding angle of the steel wire, the optimal wall thickness, and the optimal bending radius of the hose were 53.8384°, 7.31313 mm, and 164.343 mm, respectively. These parameters resulted in a minimum displacement of 1.106×10^{-3} mm. There was a 3.5% difference between the predicted and simulated values and a reduction in the displacement of 47% compared with the measured displacement of 2.18×10^{-3} mm.

In this study, the displacement caused by the coupled vibration of the fluid and hose was effectively reduced through optimization of the parameters affecting the displacement via the Taguchi experiment and the response analysis methodology. The method and results of this study will contribute to improving the working life of hydraulic hoses and provide a reference for further studies on the vibration characteristics of hydraulic pipeline systems.

References

1 J. W. Xu, Y. S. Mou, C. W. Xue, L. L. Ding, R. Y. Wang, and D. D. Ma: Energy Rep. **7** (2021) 3011. https://doi.org/10.1016/j.egyr.2021.05.035
2 A. Keramat, M. Fathi-Moghadam, R. Zanganeh, M. Rahmanshahi, A. S. Tijsseling, and E. Jabbari: J. Fluids Struct. **93** (2020) 1. https://doi.org/10.1016/j.jfluidstructs.2019.102848
3 J. H. Duan, C. J. Li, and J. Jin: Energies **15** (2022) 1. https://doi.org/10.3390/en15020670
4 M. Zagnoni, A. Golfarelli, P. Proli, S. Callegari, A. Talamelli, E. Sangiorgi, and M. Tartagni: Proc. 9th Italian Conf. (Sensors and Microsystems, 2005) 267–271.
5 J. Kutin and I. Bajsic: J. Fluids Struct. **50** (2014) 171. https://doi.org/10.1016/j.jfluidstructs.2014.05.014
6 R. Talemi, S. Cooreman, H. Mahgerefteh, S. Martynov, and S. Brown: Theor. Appl. Fract. Mech. **101** (2019) 224. https://doi.org/10.1016/j.tafmec.2019.02.005
7 F. Daude, P. Galon, and T. Douillet-Grellier: J. Fluids Struct. **101** (2021) 1. https://doi.org/10.1016/j.jfluidstructs.2021.103219
8 C. J. Zhang, X. H. Sun, Y. Y. Li, X. Q. Zhang, X. L. Zhang, X. N. Yang, and F. Li: Water **10** (2018) 1. https://doi.org/10.3390/w10101378
9 W. Qu, H. L. Zhang, W. Q. Sun, and W. Li: Compos. Struct. **255** (2021) 1. https://doi.org/10.1016/j.compstruct.2020.112958
10 SuQiangge.ProductCenter: http://chinastronger.com/product/ercenggangsibianzhiruanguanunknownEN8532SNunknown.htm (accessed December 2022).
11 D. H. Liu, X. Xia, J. Yang, and Z. W. Wang: J. Mar. Sci. Eng. **9** (2021) 1. https://doi.org/10.3390/jmse9040434
12 B. K. Shanmugam, H. Vardhan, M. G. Raj, M. Kaza, R. Sah, and H. Hanumanthappa: Int. J. Coal Prep. Util. (2022) 1. https://doi.org/10.1080/19392699.2022.2051700